Proposal for a Deterministic Single-Atom Source of Quasisuperradiant *N*-Photon Pulses

Caspar Groiseau®,[1,2] Alexander E. J. Elliott,[1,2] Stuart J. Masson,[3] and Scott Parkins[1,2,*]

[1]*Dodd-Walls Centre for Photonic and Quantum Technologies, New Zealand*
[2]*Department of Physics, University of Auckland, Auckland 1010, New Zealand*
[3]*Department of Physics, Columbia University, 538 West 120th Street, New York, New York 10027-5255, USA*

We propose a single-atom, cavity quantum electrodynamics system, compatible with recently demonstrated, fiber-integrated micro- and nanocavity setups, for the on-demand production of optical number-state, $0N$-state, and binomial-code-state pulses. The scheme makes use of Raman transitions within an entire atomic ground-state hyperfine level and operates with laser and cavity fields detuned from the atomic transition by much more than the excited-state hyperfine splitting. This enables reduction of the dynamics to that of a simple, cavity-damped Tavis-Cummings model with the collective spin determined by the total angular momentum of the ground hyperfine level.

Introduction.—Recent experiments with trapped atoms and fiber-integrated, optical micro- and nanocavities have pushed the field of cavity quantum electrodynamics (cavity QED) into a new realm of single-atom-photon coupling strengths, corresponding to unprecedentedly large single-atom cooperativities [1–6], while also offering the possibility of integrated quantum networks for quantum communication or simulation of quantum many-body systems [7–13]. A further, well-known capability provided by such large coupling strength is the generation of single photons with high fidelity through cavity-enhanced atomic spontaneous emission. Efficient single-photon sources are of course central to many efforts to realize optical quantum computation and communication.

Beyond this, however, lies an even greater, and still outstanding challenge to produce a similarly efficient source of pulses containing *exactly* N (≥ 2) optical photons. Such highly nonclassical states of light are of fundamental interest to quantum optics and constitute a starting point for the engineering of yet more complex quantum states. They are also essential for newly emerging, more resource-efficient photonic architectures for universal quantum computation and quantum error correction using individual, higher-dimensional systems [14–16] (cf. multiple two-state systems), as well as for optimal capacity of a quantum communication channel [17,18], and Heisenberg-limited quantum metrology (interferometry) [19–25].

Recent proposals and proof-of-principle demonstrations of optical N-photon sources, typically using parametric down-conversion or quantum dots, are intrinsically probabilistic and low yield in nature [26–32]. The use of a known number of (effective) two-level atoms emitting into a cavity or photonic waveguide has also been proposed [33–36], but the required many-body control and repeatability is still very challenging. Complementary to this, there also exists a range of ideas and efforts around N-photon sources in the microwave regime [37–41].

Here, we propose a deterministic N-photon source that requires just a *single* atom and makes use of its entire, multilevel energy structure in a manner that reduces the effective system dynamics to a simple and transparent form. In particular, we demonstrate that a single alkali atom coupled strongly to a cavity mode and subject to Raman transitions between sublevels of a ground F hyperfine state can replicate the collective emission of $N = 2F$ initially excited, two-level atoms into the cavity mode. In this way, a "superradiant" pulse of precisely N photons can be extracted, through the cavity mode, from a single atom. Moreover, an initial, coherent superposition state of the atom's ground sublevels is also preserved in the emission process, enabling the generation of a light pulse in an arbitrary superposition of Fock states; as particular examples, we consider the $0N$-state and binomial-code-state pulses of light.

Key to the reduction of the single-atom, multilevel dynamics is a very large detuning of the laser and cavity fields from an entire excited state hyperfine manifold of the atom, such that the excited-state hyperfine splittings can be ignored; alternatively, such that the total electronic angular momentum J is a good quantum number. Such large detuning from the atomic transition in turn demands a very large atom-cavity coupling strength and, as we show here, the experimental configurations of Refs. [1–6] attain the requisite strength for our scheme to be feasible and efficient.

The potential for making use of the multilevel energy structure of an alkali atom to prepare N-photon states has been considered previously, using either adiabatic passage with time-dependent laser and atom-cavity coupling strengths [42,43], or cavity-mediated optical pumping between atomic ground state sublevels [44,45]. However, in contrast to the present scheme, these approaches assume

near-resonant laser and cavity fields and consider just a single $F \leftrightarrow F'$ transition. This limits the range of validity of the approaches and means that Clebsch-Gordan coefficients between m_F and $m_{F'}$ sublevels play a nontrivial and restricting (with regards to choice of F and F') role in the scope and performance of the scheme.

Engineered Tavis-Cummings dynamics.—We consider a single alkali atom tightly confined inside an optical cavity. The atom couples to a π-polarized cavity mode (annihilation operator $\hat{a}$) and is also driven by either a σ_+- or σ_--polarized laser field (Fig. 1). We define the atomic dipole transition operators

$$\hat{D}_q(F, F') = \sum_{m_F=-F}^{F} |F, m_F\rangle\langle F, m_F|\mu_q|F', m_F + q\rangle$$
$$\times \langle F', m_F + q|, \quad (1)$$

where $q = \{-1, 0, 1\}$ and μ_q is the dipole operator for $\{\sigma_-, \pi, \sigma_+\}$ polarization, normalized such that $\langle\mu\rangle = 1$ for a cycling transition. The master equation for the density operator $\hat{\rho}$ of our system in the interaction picture is ($\hbar = 1$)

$$\dot{\hat{\rho}} = -i[\hat{H}_\pm, \hat{\rho}] + \kappa\mathcal{D}[\hat{a}]\hat{\rho} + \frac{\gamma}{2}\sum_q \mathcal{D}\left[\sum_{F,F'}\hat{D}_q(F, F')\right]\hat{\rho}, \quad (2)$$

where κ is the cavity field decay rate, γ the free-space atomic spontaneous emission rate, and $\mathcal{D}[\hat{O}]\hat{\rho} = 2\hat{O}\hat{\rho}\hat{O}^\dagger - \hat{\rho}\hat{O}^\dagger\hat{O} - \hat{O}^\dagger\hat{O}\hat{\rho}$. Setting the zero of energy at the lower ground hyperfine level, and assuming (for the moment) zero magnetic field, the Hamiltonian is

$$\hat{H}_\pm = \Delta_c\hat{a}^\dagger\hat{a} + \sum_{m_{F_\uparrow}}\omega_{\text{GHS}}|F_\uparrow, m_{F_\uparrow}\rangle\langle F_\uparrow, m_{F_\uparrow}|$$
$$- \sum_{F', m_{F'}}\Delta_{F'}|F', m_{F'}\rangle\langle F', m_{F'}|$$
$$+ \sum_{F,F'}\left(\frac{\Omega}{2}\hat{D}_{\pm 1}(F, F') + g\hat{a}^\dagger\hat{D}_0(F, F') + \text{H.c.}\right). \quad (3)$$

Here, $\Delta_c = \omega_c - \omega_\pm$ is the detuning between the cavity and laser frequencies, $\Omega = |\Omega|e^{i\phi}$ the Rabi frequency of the $\sigma_\pm$-polarized laser field, g the atom-cavity coupling strength, ω_{GHS} the ground state hyperfine splitting [$F_\uparrow$ ($F_\downarrow$) denotes the upper (lower) hyperfine ground state], and $\Delta_{F'} = \omega_\pm - \omega_{F'}$ the detuning of the laser from the $F_\downarrow \leftrightarrow F'$ transition. Note that, given the large coupling strengths and detunings that we consider here, we assume that the light fields couple all hyperfine ground and excited states. Consistent with this, we also assume that all atomic decays of a given polarization are into a common reservoir [46].

If we now assume also, more specifically, that the detunings of the fields (cavity and laser) are much larger than the excited state hyperfine splitting, such that this splitting can essentially be neglected, then, in addition to
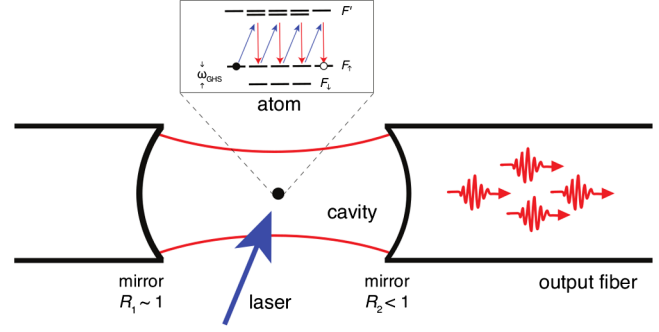

FIG. 1. Fiber-cavity configuration with a σ_+-polarized laser and π-polarized cavity mode coupled to the D_1 line of a ^{87}Rb atom. The atom is initially prepared in the $\{F = 2, m_F = -2\}$ ground-state sublevel. The cavity field decays predominantly through the right-hand mirror.

being able to adiabatically eliminate the atomic excited states and neglect atomic spontaneous emission, we obtain a tremendously simplified effective model of the atom-cavity dynamics in the form of an anti-Tavis-Cummings or Tavis-Cummings model (anti-TCM or TCM, depending on the polarization of the laser field) for a collective spin F [47–49], where F (either $F_\uparrow$ or $F_\downarrow$) is determined by the initial state of the atom; i.e., our master equation reduces to

$$\dot{\hat{\rho}} = -i[\hat{\mathcal{H}}_\pm, \hat{\rho}] + \kappa\mathcal{D}[\hat{a}]\hat{\rho}, \quad (4)$$

with

$$\hat{\mathcal{H}}_\pm = \omega\hat{a}^\dagger\hat{a} + \omega_0\hat{S}_z + \lambda(e^{-i\phi}\hat{a}\hat{S}_\mp + e^{i\phi}\hat{a}^\dagger\hat{S}_\pm), \quad (5)$$

where $\{\hat{S}_\pm, \hat{S}_z\}$ are the spin-F angular momentum operators and, for example, for the D_1 line of ^{87}Rb, the effective parameters are

$$\omega = \Delta_c + \frac{g^2}{3\Delta}, \quad \omega_0 = \omega_Z \mp \frac{|\Omega|^2}{24\Delta}, \quad \lambda = \frac{g|\Omega|}{12\sqrt{2}\Delta}. \quad (6)$$

Here, we now assume an external magnetic field giving rise to a shift ω_Z of the m_F levels. The detuning Δ depends on the choice of F; for $F = F_\uparrow$, we take $\Delta = \Delta_{F'} + \omega_{\text{GHS}}$, where the choice of F' in $\Delta_{F'}$ makes little difference due to the very large detuning assumed (in practice, we pick the lowest F'). The same forms of expressions for $\{\omega, \omega_0, \lambda\}$ are obtained for the D_1 and D_2 lines of other alkali atoms, but with slightly different numerical factors. Note that such a reduction of dynamics as described above has been demonstrated experimentally in a many-atom realization of the Dicke model with spin-1 atoms in an optical cavity [48].

The essence of our scheme follows clearly and simply from the dynamics described by Eqs. (4) and (5). With the choice $\hat{\mathcal{H}}_\pm$ and corresponding initial atom-cavity state $|F, m_F = \mp F\rangle|0\rangle_{\text{cav}}$, the system evolves irreversibly to

the unique steady state $|F, m_F = \pm F\rangle|0\rangle_{\rm cav}$ with emission from the cavity of a pulse of exactly $2F$ photons. The dynamics is irreversible because each photon that is created (via $\hat{a}^\dagger \hat{S}_\pm$) in and subsequently emitted from the cavity (at rate κ) occurs in unison with a single unidirectional step along the ladder of spin states. Additionally, in the regime of interest to us, where $\kappa \gg \sqrt{F}\lambda$ and $\omega \simeq \omega_0 \simeq 0$ (via tuning of Δ_c and ω_Z), the effective model of our *single* spin-F atom emulates resonant, cavity-mediated super-radiant emission of $2F$ spin-$\frac{1}{2}$ particles; i.e., the emitted $2F$-photon pulse will have a characteristic sech^2-shaped temporal profile [50].

Output photon number.—A preliminary way to quantify the quality of our state generation scheme is to compute the time evolution of the output photon flux from the cavity and the mean number of emitted photons, $\bar{N} = 2\kappa \int_0^\infty dt \langle \hat{a}^\dagger(t)\hat{a}(t)\rangle$. We consider first the case of a ^{87}Rb atom initially prepared in the ground state $|F = 2, m_F = -2\rangle$ and coupled to the laser and cavity fields via the D_1 line. With this system, we expect an output pulse of exactly 4 photons. Note that we neglect any extraneous photon losses, which is a good approximation provided the dominant loss channel from the system is photon transmission through the cavity mirror (at rate κ). For our quantum trajectory simulations the photon detection efficiency is additionally assumed to be ideal.

We solve the master equation numerically for the full model, Eqs. (2)–(3), and compare results with the solution for the effective anti-TCM, Eqs. (4)–(5), for two sets of cavity QED parameters: (i) $\{\kappa, g, \gamma\}/2\pi = \{50, 250, 5.7\}$ MHz and (ii) $\{\kappa, g, \gamma\}/2\pi = \{0.5, 2, 0.0057\}$ GHz. The first set corresponds to the fiber microcavity system of Refs. [1–3], while the second set is relevant to the nanocavity system of Refs. [4–6]. Results for the output photon flux are shown in Fig. 2. The agreement between the full and reduced models is clearly very good, and the predicted sech^2-shaped pulse is confirmed, with a duration on the order of $(F\lambda^2/\kappa)^{-1}$. The atomic state populations are also plotted in Fig. 2 and similarly show the expected evolution, with a smooth transfer of population along the $F = 2$ hyperfine level to the final state $|F = 2, m_F = +2\rangle$ (see Supplemental Material for further discussion [51]). A very small fraction of population may be transferred to the $F = 1$ ground state via off-resonant processes, but, in fact, the effective superradiant emission simply continues from within this level and any population there is ultimately driven back (also by an off-resonant process) into the $F = 2$ level and so to the final (dark) state $|F = 2, m_F = +2\rangle$. Atomic excited state populations are essentially negligible.

Similar results for the photon flux are shown in Fig. 3 for a ^{133}Cs atom initially prepared in the $|F = 4, m_F = -4\rangle$ ground state, also operating on the D_1 line. For the parameters used, there is a slight discrepancy between pulse shapes for the two models, but the mean photon number obtained from the full model is still very close to
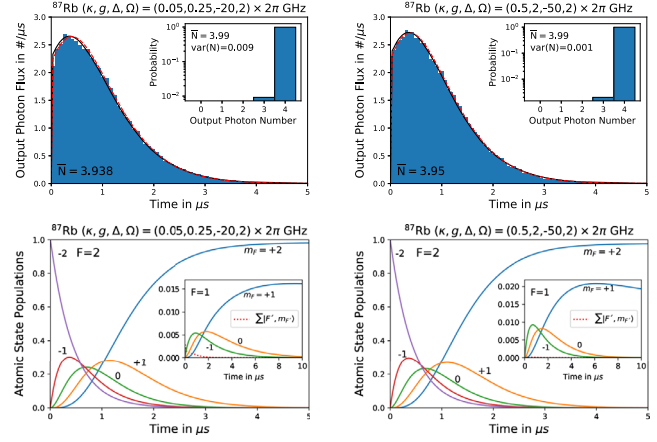

FIG. 2. Top row: Output photon flux for a ^{87}Rb atom initially prepared in $|F = 2, m_F = -2\rangle$. The black solid line represents the full model and the red dashed line the anti-TCM. The histogram shows the temporal distribution of photocounts (renormalized to $\bar{N}$) for 10 000 trajectories of the anti-TCM with additional, effective spontaneous emission. The number below the curves gives $\bar{N}$ for the full model. Insets: Histogram of photon number counts per trajectory (i.e., per output pulse). Bottom row: Atomic ground state populations ($F = 2$: main plot, $F = 1$: inset), and total excited state population (inset, red-dashed) as a function of time.

the expected value of 8. The discrepancy arises primarily from the larger excited state hyperfine splitting in ^{133}Cs, which means that a larger detuning is required to ensure closer agreement with the TCM; a similar discrepancy is also observed in ^{87}Rb for smaller detunings (see Supplemental Material [51]).

The integrated photon flux obtained from the master equation, however, does not tell us about the variance in the photon number of the output pulse. To get the variance we perform quantum trajectory simulations [58,59] and record the times and total number of photon counts in each trajectory. The histogram of photon detection times gives us again the output photon flux, which is shown for comparison in Figs. 2 and 3, along with the photon number distribution and its variance for the output pulse. The distributions are clearly very close to an ideal number state. Note that for these simulations we do not use the full model (owing to the stiffness of the numerical integration caused by the large detunings and ground state hyperfine splitting), but rather use the anti-TCM (or TCM) with spontaneous emission added, in the form of an effective Lindblad operator acting just within the relevant ground state (see Supplemental Material [51]). Spontaneous emission to the other hyperfine ground state is therefore neglected, but the numerical results from the master equation support this as a good approximation.

Finally, we note that shorter or longer output pulses can be obtained by changing the detuning Δ and/or laser Rabi frequency Ω. Also, in the results presented here, we assume
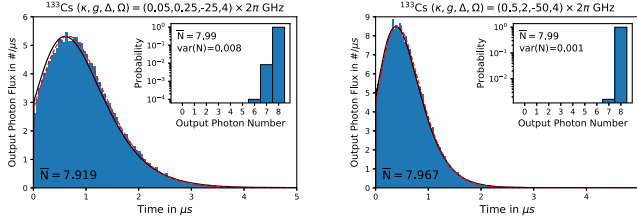
FIG. 3. Output photon flux for a ^{133}Cs atom initially prepared in $|F = 4, m_F = -4\rangle$. Line markings, histograms, and annotations are the same as described in Fig. 2.

an instantaneous switch-on of the laser field. This can be relaxed to allow for a smooth initial ramp of the laser field to its peak value, which can be used to tailor the shape of the output $2F$-photon pulse (see the Supplemental Material [51] for additional examples).

0N-states and other superpositions.—Instead of starting with an atom in an end state of the Zeeman ladder, we also have the option to start with a superposition of Zeeman substates; for example, $|\psi_{\text{oat}}\rangle_F = (|F, -F\rangle + |F, +F\rangle)/\sqrt{2}$, which can be created using a one-axis twisting (oat) scheme [60], or an arbitrary superposition, created using a scheme such as in Ref. [61]. With our proposed system, these atomic superposition states are directly mapped onto photonic states of the output light pulse. So, for example, the initial state $|\psi_{\text{oat}}\rangle_F$ leads to an output pulse in a coherent superposition of vacuum and $N = 2F$ photons, i.e., a $0N$-state, $|\Psi\rangle_{\text{pulse}} = (|0\rangle_{\text{out}} + |N\rangle_{\text{out}})/\sqrt{2}$, which is a basic resource in schemes proposed for universal quantum computation [14]. The output photon flux and photon number distribution for initial atomic state $|\psi_{\text{oat}}\rangle_{F=2}$ are shown in Fig. 4 for ^{87}Rb with cavity QED parameters relevant to the fiber microcavity.

As a further example, in Fig. 4 we also consider an initial state of ^{87}Rb of the form $|\psi_{\text{bc}}\rangle_{F=2} = (|2, -2\rangle + \sqrt{2}|2, 0\rangle + |2, +2\rangle)/2$, yielding an output pulse state $|\Psi\rangle_{\text{pulse}} = (|0\rangle_{\text{out}} + \sqrt{2}|2\rangle_{\text{out}} + |4\rangle_{\text{out}})/2$. Such a state is of particular interest, as it constitutes a superposition of states $|0_L\rangle = (|0\rangle + |4\rangle)/\sqrt{2}$ and $|1_L\rangle = |2\rangle$, which are logically encoded (binomial code) states of a qubit for a quantum
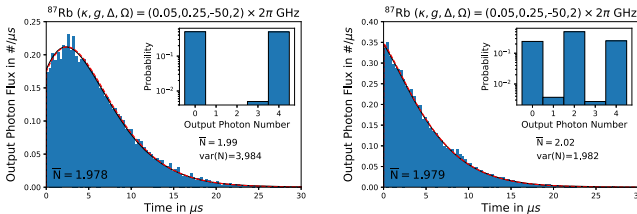
computation scheme protected up to one photon loss [15]. Note that in mapping general atomic ground-state superpositions onto the states of the output light pulses, one must pay attention to the relative phases between the different components and the phase ϕ of the effective cavity-spin coupling. For an exact mapping of relative phases, we require in our model that $\phi = \mp \pi/2$ (depending on the sign of Δ), which can of course be chosen through the phase of the laser field (see Supplemental Material [51]). Alternatively, ϕ can also be incorporated as the relative phase between neighbouring m_F levels in the initial atomic state.

Quantum state tomography.—The photon number distribution of the output pulse is not sufficient to confirm that the desired output state has been generated. To verify that the target quantum state has indeed been generated, we implement quantum state tomography on simulated, pulsed-homodyne measurements, obtained via the method of homodyne quantum trajectories (see Supplemental Material [51]). That is, we reconstruct the Wigner function of the pulse by measuring marginals of the Wigner function for a set of homodyne phase angles θ and then applying the inverse Radon transform to these marginals [62]. For these simulations, we again use the TCM with effective spontaneous emission added. Results of these reconstructions are shown in Fig. 5. Our reconstructions can clearly be assigned to the predicted, ideal state. For a better
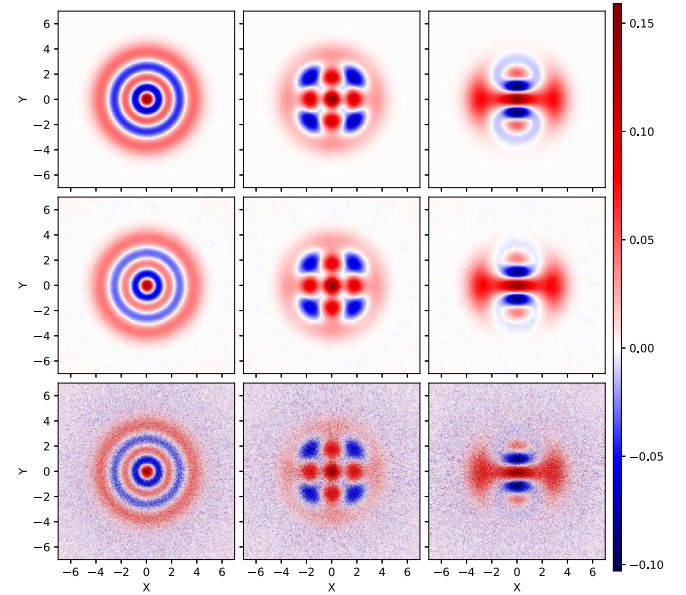

FIG. 5. Top row: Wigner functions of the states (left to right) $|4\rangle$, $(|0\rangle + |4\rangle)/\sqrt{2}$, and $(|0\rangle + \sqrt{2}|2\rangle + |4\rangle)/2$. Bottom row: raw reconstructed Wigner functions of the cavity output pulses for a single ^{87}Rb atom in a fiber microcavity setup ($\{\kappa, g, \Delta, \Omega\} = \{0.05, 0.25, -50, 2\} \cdot 2\pi$ GHz) with initial atomic states (left to right) $|2, -2\rangle$, $|\psi_{\text{oat}}\rangle_{F=2}$, and $|\psi_{\text{bc}}\rangle_{F=2}$. The reconstructions are using a set of 500 angles $\theta \in [0, \pi)$ and 10 000 trajectories per angle. Middle row: Simulated reconstructions smoothed by a Gaussian blur.

FIG. 4. Output photon flux for a ^{87}Rb atom initially prepared in the states $|\psi_{\text{oat}}\rangle_{F=2}$ (left) and $|\psi_{\text{bc}}\rangle_{F=2}$ (right). Line markings, histograms, and annotations are the same as described in Fig. 2. Note the larger detuning used here, which leads to a slower timescale than in Fig. 2.

comparison, we remove most of the noise from the simulated results by smoothing with a Gaussian blur, which reveals some discrepancy in the heights of the maxima and minima between the ideal case and our reconstruction. This effect can also be observed in the untreated marginals, where we observe some noise in the outer peaks of these marginals that can be attributed to atomic spontaneous emission.

Alternatively, the density matrix itself can be reconstructed using maximum likelihood estimation [63,64] on the marginals, or using the input-output formalism for quantum pulses [65]. Doing so allows a direct comparison with the target states and we obtain fidelities in excess of 90% (see Supplemental Material [51]).

Conclusion and outlook.—We have proposed a single-atom, deterministic source of optical number-state, $0N$-state, and binomial-code-state pulses. The scheme does not require time-dependent atom-laser or atom-cavity coupling strengths or detunings, or specific $F \leftrightarrow F'$ atomic transitions, and should be feasible with recently demonstrated, fiber-integrated micro- and nanocavity QED setups. Some other potential features of the scheme are worth noting. For the case of number-state pulses, it is a simple matter to generate a stream of separate pulses by switching the polarization of the laser field at the end of each pulse and cycling the atom back and forth between the end states $|F, \pm m_F\rangle$. Also, one may increase the number of photons per pulse N by adding more atoms; e.g., with two identically prepared ^{87}Rb atoms coupled collectively to the cavity mode, the effective spin in the TCM is simply doubled, enabling the generation of eight-photon pulses. Finally, we have assumed throughout this work that the cavity is essentially one-sided, so that pulses are emitted in just one direction into the output fiber. We could equally well assume a symmetric cavity, in which case our scheme could be equated to a 50-50 beam splitter with the incident state in one input port determined by the initial state of the atom. This would provide a straightforward means of producing an entangled state of light fields propagating in opposite directions away from the cavity.

---

*s.parkins@auckland.ac.nz

[1] R. Gehr, J. Volz, G. Dubois, T. Steinmetz, Y. Colombe, B. L. Lev, R. Long, J. Estève, and J. Reichel, Cavity-Based Single Atom Preparation and High-Fidelity Hyperfine State Read-out, Phys. Rev. Lett. **104**, 203602 (2010).

[2] F. Haas, J. Volz, R. Gehr, J. Reichel, and J. Estève, Entangled states of more than 40 atoms in an optical fiber cavity, Science **344**, 180 (2014).

[3] G. Barontini, L. Hohmann, F. Haas, J. Estève, and J. Reichel, Deterministic generation of multiparticle entanglement by quantum Zeno dynamics, Science **349**, 1317 (2015).

[4] J. D. Thompson, T. G. Tiecke, N. P. de Leon, J. Feist, A. V. Akimov, M. Gullans, A. S. Zibrov, V. Vuletić, and M. D. Lukin, Coupling a single trapped atom to a nanoscale optical cavity, Science **340**, 1202 (2013).

[5] T. G. Tiecke, J. D. Thompson, N. P. de Leon, L. R. Liu, V. Vuletić, and M. D. Lukin, Nanophotonic quantum phase switch with a single atom, Nature (London) **508**, 241 (2014).

[6] P. Samutpraphoot, T. Đorđević, P. L. Ocola, H. Bernien, C. Senko, V. Vuletić, and M. D. Lukin, Strong Coupling of Two Individually Controlled Atoms via a Nanophotonic Cavity, Phys. Rev. Lett. **124**, 063602 (2020).

[7] S.-H. Tan and P. P. Rohde, The resurgence of the linear optics quantum interferometer—recent advances and applications, Rev. Phys. **4**, 100030 (2019).

[8] S. Slussarenko and G. J. Pryde, Photonic quantum information processing: A concise review, Appl. Phys. Rev. **6**, 041303 (2019).

[9] F. Flamini, N. Spagnolo, and F. Sciarrino, Photonic quantum information processing: A review, Rep. Prog. Phys. **82**, 016001 (2019).

[10] J. L. O'Brien, A. Furusawa, and J. Vučković, Photonic quantum technologies, Nat. Photonics **3**, 687 (2009).

[11] P. Kok, W. J. Munro, K. Nemoto, T. C. Ralph, J. P. Dowling, and G. J. Milburn, Linear optical quantum computing with photonic qubits, Rev. Mod. Phys. **79**, 135 (2007).

[12] H. J. Kimble, The quantum internet, Nature (London) **453**, 1023 (2008).

[13] J. L. O'Brien, Optical quantum computing, Science **318**, 1567 (2007).

[14] K. K. Sabapathy and C. Weedbrook, ON states as resource units for universal quantum computation with photonic architectures, Phys. Rev. A **97**, 062315 (2018).

[15] M. H. Michael, M. Silveri, R. T. Brierley, V. V. Albert, J. Salmilehto, L. Jiang, and S. M. Girvin, New Class of Quantum Error-Correcting Codes for a Bosonic Mode, Phys. Rev. X **6**, 031006 (2016).

[16] L. Hu, Y. Ma, W. Cai, X. Mu, Y. Xu, W. Wang, Y. Wu, H. Wang, Y. P. Song, C.-L. Zou *et al.*, Quantum error correction and universal gate set operation on a binomial bosonic logical qubit, Nat. Phys. **15**, 503 (2019).

[17] Y. Yamamoto and H. A. Haus, Preparation, measurement and information capacity of optical quantum states, Rev. Mod. Phys. **58**, 1001 (1986).

[18] C. M. Caves and P. D. Drummond, Quantum limits on bosonic communication rates, Rev. Mod. Phys. **66**, 481 (1994).

[19] S. Slussarenko, M. M. Weston, H. M. Chrzanowski, L. K. Shalm, V. B. Verma, S. W. Nam, and G. J. Pryde, Unconditional violation of the shot-noise limit in photonic quantum metrology, Nat. Photonics **11**, 700 (2017).

[20] J.-W. Pan, Z.-B. Chen, C.-Y. Lu, H. Weinfurter, A. Zeilinger, and M. Żukowski, Multiphoton entanglement and interferometry, Rev. Mod. Phys. **84**, 777 (2012).

[21] T. Nagata, R. Okamoto, J. L. O'Brien, K. Sasaki, and S. Takeuchi, Beating the standard quantum limit with four-entangled photons, Science **316**, 726 (2007).

[22] M. W. Mitchell, J. S. Lundeen, and A. M. Steinberg, Super-resolving phase measurements with a multiphoton entangled state, Nature (London) **429**, 161 (2004).

[23] L. Pezzé and A. Smerzi, Ultrasensitive Two-Mode Interferometry with Single-Mode Number Squeezing, Phys. Rev. Lett. **110**, 163604 (2013).

[24] R. A. Campos, C. C. Gerry, and A. Benmoussa, Optical interferometry at the Heisenberg limit with twin Fock states and parity measurements, Phys. Rev. A **68**, 023810 (2003).

[25] M. J. Holland and K. Burnett, Interferometric Detection of Optical Phase Shifts at the Heisenberg Limit, Phys. Rev. Lett. **71**, 1355 (1993).

[26] C. S. Muñoz, E. Del Valle, A. G. Tudela, K. Müller, S. Lichtmannecker, M. Kaniber, C. Tejedor, J. J. Finley, and F. P. Laussy, Emitters of N-photon bundles, Nat. Photonics **8**, 550 (2014).

[27] E. Waks, E. Diamanti, and Y. Yamamoto, Generation of photon number states, New J. Phys. **8**, 4 (2006).

[28] S. Krapick, B. Brecht, H. Herrmann, V. Quiring, and C. Silberhorn, On-chip generation of photon-triplet states, Opt. Express **24**, 2836 (2016).

[29] M. G. Moebius, F. Herrera, S. Griesse-Nascimento, O. Reshef, C. C. Evans, G. G. Guerreschi, A. Aspuru-Guzik, and E. Mazur, Efficient photon triplet generation in integrated nanophotonic waveguides, Opt. Express **24**, 9932 (2016).

[30] K. A. Fischer, L. Hanschke, J. Wierzbowski, T. Simmet, C. Dory, J. J. Finley, J. Vučković, and K. Müller, Signatures of two-photon pulses from a quantum two-level system, Nat. Phys. **13**, 649 (2017).

[31] M. Khoshnegar, T. Huber, A. Predojević, D. Dalacu, M. Prilmüller, J. Lapointe, X. Wu, P. Tamarat, B. Lounis, P. Poole et al., A solid state source of photon triplets based on quantum dot molecules, Nat. Commun. **8**, 15716 (2017).

[32] J. C. Loredo, C. Antón, B. Reznychenko, P. Hilaire, A. Harouri, C. Millet, H. Ollivier, N. Somaschi, L. De Santis, A. Lemaître et al., Generation of non-classical light in a photon-number superposition, Nat. Photonics **13**, 803 (2019).

[33] K. R. Brown, K. M. Dani, D. M. Stamper-Kurn, and K. B. Whaley, Deterministic optical Fock-state generation, Phys. Rev. A **67**, 043818 (2003).

[34] A. González-Tudela, V. Paulisch, D. E. Chang, H. J. Kimble, and J. I. Cirac, Deterministic Generation of Arbitrary Photonic States Assisted by Dissipation, Phys. Rev. Lett. **115**, 163603 (2015).

[35] A. González-Tudela, V. Paulisch, H. J. Kimble, and J. I. Cirac, Efficient Multiphoton Generation in Waveguide Quantum Electrodynamics, Phys. Rev. Lett. **118**, 213601 (2017).

[36] V. Paulisch, M. Perarnau-Llobet, A. González-Tudela, and J. I. Cirac, Quantum metrology with one-dimensional super-radiant photonic states, Phys. Rev. A **99**, 043807 (2019).

[37] V. S. C. Canela and H. J. Carmichael, Bright Sub-Poissonian Light through Intrinsic Feedback and External Control, Phys. Rev. Lett. **124**, 063604 (2020).

[38] M. Uria, P. Solano, and C. Hermann-Avigliano, Deterministic Generation of Large Fock States, Phys. Rev. Lett. **125**, 093603 (2020).

[39] M. Hofheinz, E. M. Weig, M. Ansmann, R. C. Bialczak, E. Lucero, M. Neeley, A. D. O'connell, H. Wang, J. M. Martinis, and A. N. Cleland, Generation of Fock states in a superconducting quantum circuit, Nature (London) **454**, 310 (2008).

[40] S. P. Premaratne, F. C. Wellstood, and B. S. Palmer, Micro-wave photon Fock state generation by stimulated Raman adiabatic passage, Nat. Commun. **8**, 14148 (2017).

[41] C. Sayrin, I. Dotsenko, X. Zhou, B. Peaudecerf, T. Rybarczyk, S. Gleyzes, P. Rouchon, M. Mirrahimi, H. Amini, M. Brune, J.-M. Raimond, and S. Haroche, Real-time quantum feedback prepares and stabilizes photon number states, Nature (London) **477**, 73 (2011).

[42] A. S. Parkins, P. Marte, P. Zoller, and H. J. Kimble, Synthesis of Arbitrary Quantum States via Adiabatic Transfer of Zeeman Coherence, Phys. Rev. Lett. **71**, 3095 (1993).

[43] A. S. Parkins, P. Marte, P. Zoller, O. Carnal, and H. J. Kimble, Quantum-state mapping between multilevel atoms and cavity light fields, Phys. Rev. A **51**, 1578 (1995).

[44] A. Gogyan, S. Guérin, C. Leroy, and Yu. Malakyan, Deterministic production of n-photon states from a single atom-cavity system, Phys. Rev. A **86**, 063801 (2012).

[45] A. Gogyan and Yu. Malakyan, Deterministic quantum state transfer between remote atoms with photon-number super-position states, Phys. Rev. A **98**, 052304 (2018).

[46] K. M. Birnbaum, A. S. Parkins, and H. J. Kimble, Cavity QED with multiple hyperfine levels, Phys. Rev. A **74**, 063802 (2006).

[47] S. J. Masson, M. D. Barrett, and S. Parkins, Cavity QED Engineering of Spin Dynamics and Squeezing in a Spinor Gas, Phys. Rev. Lett. **119**, 213601 (2017).

[48] Z. Zhiqiang, C. H. Lee, R. Kumar, K. J. Arnold, S. J. Masson, A. S. Parkins, and M. D. Barrett, Nonequilibrium phase transition in a spin-1 Dicke model, Optica **4**, 424 (2017).

[49] S. J. Masson and S. Parkins, Rapid Production of Many-Body Entanglement in Spin-1 Atoms via Cavity Output Photon Counting, Phys. Rev. Lett. **122**, 103601 (2019).

[50] J. H. Eberly, Superradiance revisited, Am. J. Phys. **40**, 1374 (1972).

[51] See Supplemental Material at http://link.aps.org/supplemental/10.1103/PhysRevLett.127.033602 for additional information on the state populations, alternative parameters, some of the methods used for the simulation of the system, and the quantum state reconstruction, which includes Refs. [52–57].

[52] F. Reiter and A. S. Sørensen, Effective operator formalism for open quantum systems, Phys. Rev. A **85**, 032111 (2012).

[53] H. J. Carmichael, Statistical Methods in Quantum Optics 2: Non-Classical Fields (Springer Science & Business Media, New York, 2009).

[54] H. P. Yuen and V. W. S. Chan, Noise in homodyne and heterodyne detection, Opt. Lett. **8**, 177 (1983).

[55] M. G. Raymer and I. Walmsley, Temporal modes in quantum optics: Then and now, Phys. Scr. **95**, 064002 (2020).

[56] C. W. Gardiner, Driving a Quantum System with the Output Field from Another Driven Quantum System, Phys. Rev. Lett. **70**, 2269 (1993).

[57] H. J. Carmichael, Quantum Trajectory Theory for Cascaded Open Systems, Phys. Rev. Lett. **70**, 2273 (1993).

[58] H. Carmichael, *An Open Systems Approach to Quantum Optics* (Springer, Berlin Heidelberg, 1993), Bd. 18.

[59] K. Mølmer, Y. Castin, and J. Dalibard, Monte Carlo wave-function method in quantum optics, J. Opt. Soc. Am. B **10,** 524 (1993).

[60] T. Chalopin, C. Bouazza, A. Evrard, V. Makhalov, D. Dreon, J. Dalibard, L. A. Sidorenkov, and S. Nascimbene, Quantum-enhanced sensing using non-classical spin states of a highly magnetic atom, Nat. Commun. **9,** 4955 (2018).

[61] C. K. Law and J. H. Eberly, Synthesis of arbitrary super-position of Zeeman states in an atom, Opt. Express **2,** 368 (1998).

[62] K. Vogel and H. Risken, Determination of quasiprobability distributions in terms of probability distributions for the rotated quadrature phase, Phys. Rev. A **40,** 2847 (1989).

[63] Z. Hradil, Quantum-state estimation, Phys. Rev. A **55,** R1561 (1997).

[64] A. I. Lvovsky, Iterative maximum-likelihood reconstruction in quantum homodyne tomography, J. Opt. B **6,** S556 (2004).

[65] A. H. Kiilerich and K. Mølmer, Input-Output Theory with Quantum Pulses, Phys. Rev. Lett. **123,** 123604 (2019).

[66] J. R. Johansson, P. D. Nation, and F. Nori, QuTiP: An open-source Python framework for the dynamics of open quantum systems, Comput. Phys. Commun. **183,** 1760 (2012).

[67] J. R. Johansson, P. D. Nation, and F. Nori, QuTiP 2: A Python framework for the dynamics of open quantum systems, Comput. Phys. Commun. **184,** 1234 (2013).